Effect of material properties on the accuracy of antiresonant approximation: Linear and second-order optical responses

Nicolas Tancogne-Dejean,[1,2,*] Bernardo S. Mendoza,[3] and Valérie Véniard[1,2]
[1]*Laboratoire des Solides Irradiés, École Polytechnique, CNRS, CEA/DSM, 91128 Palaiseau, France*
[2]*European Theoretical Spectroscopy Facility (ETSF), Palaiseau, France*
[3]*Centro de Investigaciones en Óptica, León, Guanajuato, México*
(Received 24 April 2014; revised manuscript received 16 July 2014; published 29 July 2014)

Many *ab initio* calculations, in particular in solid state physics, rely on the antiresonant approximation. In this paper we discuss the derivation, the validity, and the accuracy of this approximation, analyzing how the optical properties of several bulk semiconducting materials and surfaces can be affected. We present accurate results for different spectroscopic quantities in the linear and nonlinear responses and we analyze the discrepancies between approximated and exact formulas. An investigation is made of the effect of the approximation on absorption spectra for different materials, showing the reliability of the approximation even in the presence of local field and excitonic effects. The energy loss is shown to be drastically affected. The effect of the band gap of materials on the quality of the approximation is also discussed. Finally, we report on the influence of the antiresonant approximation on second harmonic generation spectra.

DOI: 10.1103/PhysRevB.90.035212 PACS number(s): 71.10.−w, 78.20.−e, 71.15.Ap

I. INTRODUCTION

Optical spectroscopies are widespread in many fields of science, such as physics [1], chemistry [2,3], and biology [4]. Linear and nonlinear spectroscopies give valuable information on the structural and electronic properties of materials. Experimental and theoretical approaches have considerably advanced over the last years deepening our understanding of the processes occurring in condensed matter. Traditional linear spectroscopies, such as absorption or electron energy loss, rely on the knowledge of the dielectric tensor and the number of *ab initio* calculations of electronic spectra has increased impressively. Many of these calculations are based on density-functional theory (DFT) and imply a summation over a large number of valence and conduction states [5–7]. On the other hand, nonlinear spectroscopies represent an attractive alternative to linear spectroscopies. A lot of effort as been devoted recently for finding nonlinear crystals [8,9] or for describing effects, e.g., Kerr effect [10,11].

Among all the nonlinear processes, second harmonic generation (SHG) is considered as a versatile tool to study many kinds of surfaces [12–14], interfaces [15,16], and nanostructures [17–19]. The theoretical description of the phenomena is well established and gives reliable results [20–22], but the numerical evaluation of the associated susceptibilities is a nontrivial task, which limits its application to relatively simple systems. The huge computational effort required, even with nowadays computer facilities, explains the need for reliable approximations that could speed up the numerical evaluation and allow the study of complex large-scale systems.

One of the most commonly used approximation in linear calculations is the so-called antiresonant approximation (AA), in which the first order response is split into two terms, the resonant and the nonresonant contributions, the latter being neglected in the response functions [23]. The success of this approximation relies on its simplicity and ease of implementation for the calculation of linear response. However, its derivation for the second-order susceptibility is more intricate and has not been mentioned up to now.

Note that this approximation is different from the Tamm-Dancoff approximation, used in the framework of the Bethe-Salpeter equation [5] or for the Casidas linear response [24], where only the coupling between the resonant and antiresonant contributions is neglected in the Hamiltonian. In this article we exemplify what are the consequences of neglecting the antiresonant terms in the calculation of the optical response at different levels of approximation. We investigate the AA for the linear and the nonlinear optical responses. Our goal is to provide criteria for determining the range of validity of the approximation. We show, in particular, that the success of the approximation depends strongly on the physical quantity we want to calculate and we find that this approximation is more suitable for some spectroscopies than others.

For the sake of generality, we will study both bulk materials and surfaces. Thus, as examples we have chosen cubic bulk semiconductor crystals and two semiconducting surfaces. For the surfaces we have chosen the clean Si(001)2×1 and the dihydride Si(001)1×1:2H. The clean surface is characterized by asymmetric dimers formed between the two topmost Si atoms, resulting in a very small gap (E_g) due to surface states. On the other hand, the hydrogenated surface is a bulk-terminated surface where hydrogen saturates all the dangling bonds, suppressing all the surface states, leading to a larger gap.

The paper is organized as follows. In Sec. II we present the antiresonant approximation for the dielectric response $\epsilon_{ab}(\omega)$ and the second-order susceptibility $\chi_{abc}(\omega)$. Then, in Sec. III we present the comparison of the AA with the full calculation, where both resonant and antiresonant terms are included. We present accurate results for linear spectroscopies, namely absorption and energy loss spectra. We stress the influence of the local field and excitonic effects on the AA spectra. The effect on surface spectroscopies is presented through reflectance anisotropy spectra. Finally, we analyze the role of

*nicolas.tancogne-dejean@polytechnique.edu

the approximation on the second harmonic generation spectra. We give our conclusions in Sec. IV.

II. ANTIRESONANT APPROXIMATION

A. Linear response

Within the independent particle approximation (IPA) the dielectric function of a bulk crystal is given by [25]

$$\epsilon_{ab}(\omega) = \delta_{ab} + \frac{8\pi e^2}{\hbar V}\sum_{mn\mathbf{k}} \frac{f_{nm}(\mathbf{k}) v^a_{nm}(\mathbf{k}) v^b_{mn}(\mathbf{k})}{\omega^2_{mn}(\mathbf{k})[\omega_{mn}(\mathbf{k}) - \tilde{\omega}]}, \quad (1)$$

where e is the charge of the electron, and $f_{nm}(\mathbf{k}) = f_n(\mathbf{k}) - f_m(\mathbf{k})$, with $f_n(\mathbf{k})$ the Fermi occupation number of the Bloch state $|n\mathbf{k}\rangle$ with the energy $E_{n\mathbf{k}}$ at point $\mathbf{k}$. For temperature $T = 0$ K, $f_n(\mathbf{k}) = f_n = 1$, where n corresponds to a valence (v) band and 0 where n corresponds to a conduction (c) band. Also, V is the volume of the crystal, $\tilde{\omega} = \omega + i\eta$ is the angular frequency with a small positive imaginary part η, that turns on (adiabatically) the electromagnetic field $\hbar\omega_{mn} = E_{nm\mathbf{k}} - E_{mn\mathbf{k}}$, and $v^a_{nm}(\mathbf{k}) = \langle n\mathbf{k}|\hat{v}^a|m\mathbf{k}\rangle$ is a velocity matrix element. The sum over $\mathbf{k}$ is restricted to the first Brillouin zone. Finally, the spin degeneracy is accounted for in the prefactor of the sum.

In order to make self-evident the antiresonant terms of Eq. (1), we separate the sum over n and m into $v \to c$ and $c \to v$ transitions, i.e.,

$$\epsilon_{ab}(\omega) = \delta_{ab} + \frac{8\pi e^2}{\hbar V}\sum_{vc\mathbf{k}} \left[\frac{v^a_{vc}(\mathbf{k}) v^b_{cv}(\mathbf{k})}{\omega^2_{cv}[\omega_{cv}(\mathbf{k}) - \tilde{\omega}]} - \frac{v^a_{cv}(\mathbf{k}) v^b_{vc}(\mathbf{k})}{\omega^2_{vc}[\omega_{vc}(\mathbf{k}) - \tilde{\omega}]}\right]. \quad (2)$$

Considering only positive ω for $\epsilon_{ab}(\omega)$, we immediately see that in the above equation the leading term is the one containing $1/[\omega_{cv}(\mathbf{k}) - \tilde{\omega}]$ because as $\hbar\omega_{cv}(\mathbf{k})$ is a positive energy the term will diverge as $\omega \to \omega_{cv}(\mathbf{k})$. Thus, as discussed in the Introduction, we call this term resonant. On the other hand, the term proportional to $1/[\omega_{vc}(\mathbf{k}) - \tilde{\omega}]$ will not diverge as $\omega \to \omega_{vc}(\mathbf{k})$ since now $\hbar\omega_{vc}(\mathbf{k})$ is a negative energy. Consequently, we call this term antiresonant. Therefore, the antiresonant approximation (AA) to $\epsilon_{ab}(\omega)$ [23] results when we neglect the antiresonant term in Eq. (2), i.e.,

$$\epsilon^{\mathrm{AA}}_{ab}(\omega) = \delta_{ab} + \frac{8\pi e^2}{\hbar V}\sum_{cv\mathbf{k}} \frac{v^a_{vc}(\mathbf{k}) v^b_{cv}(\mathbf{k})}{\omega^2_{cv}[\omega_{cv}(\mathbf{k}) - \tilde{\omega}]}. \quad (3)$$

In the independent particle approximation, two major contributions to the dielectric function have been neglected, namely local field and many-body effects. The inclusion of such effects can be done in the framework of the time-dependent density functional theory (TDDFT). The quantity that governs the optical properties of the crystal in that case is the macroscopic dielectric function ϵ_M, directly related to microscopic dielectric matrix $\epsilon(\mathbf{q}+\mathbf{G},\mathbf{q}+\mathbf{G}';\omega)$. Here $\mathbf{q}$ denotes a vanishing wave vector and $\mathbf{G}$,$\mathbf{G}'$ are reciprocal lattice vectors of the crystal. The longitudinal part of the dielectric matrix is given by

$$\epsilon_M(\mathbf{q};\omega) = \lim_{\mathbf{q}\to 0} \frac{1}{\epsilon^{-1}(\mathbf{q}+\mathbf{G},\mathbf{q}+\mathbf{G}';\omega)}\bigg|_{\mathbf{G}=\mathbf{G}'=0}. \quad (4)$$

The inverse of the microscopic dielectric matrix is given by $\epsilon^{-1}(\mathbf{q}+\mathbf{G},\mathbf{q}+\mathbf{G}';\omega) = \delta_{\mathbf{GG}'} + v(\mathbf{q}+\mathbf{G})\chi_{\mathbf{GG}'}(\mathbf{q};\omega)$, with $v(\mathbf{q}+\mathbf{G}) = 4\pi e^2/|\mathbf{q}+\mathbf{G}|^2$ and χ is the fully interacting susceptibility. In frequency and reciprocal space, one has to solve a Dyson-like matrix equation for obtaining $\chi_{\mathbf{GG}'}(\mathbf{q};\omega)$ [25],

$$\chi_{\mathbf{GG}'}(\mathbf{q};\omega) = \chi^{(0)}_{\mathbf{GG}'}(\mathbf{q};\omega) + \sum_{\mathbf{G}''\mathbf{G}'''} \chi^{(0)}_{\mathbf{GG}''} \times (\mathbf{q};\omega)(v + f_{\mathrm{xc}})_{\mathbf{G}''\mathbf{G}'''}(\mathbf{q};\omega)\chi_{\mathbf{G}'''\mathbf{G}'}(\mathbf{q};\omega). \quad (5)$$

Here f_{xc} is the exchange and correlation (xc) kernel and $\chi^{(0)}_{\mathbf{GG}'}(\mathbf{q};\omega)$ is the noninteracting susceptibility defined by

$$\chi^{(0)}_{\mathbf{GG}''}(\mathbf{q};\omega) = \frac{2}{\hbar V}\sum_{mn\mathbf{k}}(f_n(\mathbf{k}) - f_m(\mathbf{k}+\mathbf{q})) \times \frac{\langle n,\mathbf{k}|e^{-i(\mathbf{q}+\mathbf{G})\mathbf{r}}|m,\mathbf{k}+\mathbf{q}\rangle\langle m,\mathbf{k}+\mathbf{q}|e^{i(\mathbf{q}+\mathbf{G}')\mathbf{r}}|n,\mathbf{k}\rangle}{[\tilde{\omega} - \omega_{mn}(\mathbf{k})]}. \quad (6)$$

The AA will be obtained by replacing $\chi^{(0)}$ by $\chi^{(0)\mathrm{AA}}$, as presented above for ϵ_{ab} in the independent particle approximation.

In this paper we will focus on two approximations for f_{xc}. The first one is the random phase approximation (RPA) and corresponds to $f_{\mathrm{xc}} = 0$. It allows us to take into account local field effects. The second one is the so-called "long-range kernel" [6] approximation, where f_{xc} is approximated by $-\alpha/q^2$, where α is a mean value for the dynamical dependence of f_{xc} in a given range of energy. If used on top of a GW or a scissors correction of the band structure, it has been shown to simulate correctly excitons for a large variety of semiconductors [6]. More sophisticated kernels exist, but they are beyond the scope of this paper, as our goal is to discuss the effect of the AA when the exciton is included in the calculations.

B. Second-order response

To obtain the second harmonic susceptibility tensor $\chi_{abc}(-2\omega;\omega,\omega)$ in the antiresonant approximation, we start from the independent particle expression of Ref. [26], where χ_{abc} is split into two and three bands contributions so that $\chi_{abc}(-2\omega;\omega,\omega) = \chi^{2\mathrm{band}}_{abc}(-2\omega;\omega,\omega) + \chi^{3\mathrm{band}}_{abc}(-2\omega;\omega,\omega)$, where

$$\chi^{2\mathrm{band}}_{abc} = \frac{ie^3}{\hbar^2 V}\sum_{mn\mathbf{k}} \frac{f_{nm}(\mathbf{k}) v^a_{nm}(\mathbf{k})\{v^b_{mn}(\mathbf{k})\Delta^c_{mn}(\mathbf{k})\}}{\omega^4_{mn}(\mathbf{k})} \times\left[\frac{16}{[\omega_{mn}(\mathbf{k}) - 2\tilde{\omega}]} - \frac{1}{[\omega_{mn}(\mathbf{k}) - \tilde{\omega}]}\right] \quad (7)$$

and

$$\chi^{3\mathrm{band}}_{abc} = \frac{ie^3}{\hbar^2 V}\sum_{mnl}\sum_{\mathbf{k}} \frac{v^a_{nm}(\mathbf{k})\{v^b_{ml}(\mathbf{k})v^c_{ln}(\mathbf{k})\}}{[2\omega_{ln}(\mathbf{k}) - \omega_{ml}(\mathbf{k})]} \times\left[\frac{16 f_{nm}(\mathbf{k})}{\omega^3_{mn}(\mathbf{k})[\omega_{mn}(\mathbf{k}) - 2\tilde{\omega}]} + \frac{f_{ln}(\mathbf{k})}{\omega^3_{ln}(\mathbf{k})[\omega_{ln}(\mathbf{k}) - \tilde{\omega}]} + \frac{f_{ml}(\mathbf{k})}{\omega^3_{lm}(\mathbf{k})[\omega_{ml}(\mathbf{k}) - \tilde{\omega}]}\right]. \quad (8)$$

We omit the frequency dependence in χ_{abc} from now on to simplify the notation. In the above expressions,

$$\left\{v^b_{ml}(\mathbf{k})v^c_{ln}(\mathbf{k})\right\} = \tfrac{1}{2}\left[v^b_{ml}(\mathbf{k})v^c_{ln}(\mathbf{k}) + v^c_{ml}(\mathbf{k})v^b_{ln}(\mathbf{k})\right] \quad (9)$$

results from the symmetrization of the last two Cartesian indices required for having $\chi_{abc} = \chi_{acb}$ and $\Delta^b_{mn}(\mathbf{k}) = v^b_{mm}(\mathbf{k}) - v^b_{nn}(\mathbf{k})$, where $v^b_{mm}(\mathbf{k}) = \langle m\mathbf{k}|\hat{v}^b|m\mathbf{k}\rangle$ is a velocity matrix element. As for the linear case expression, the spin degeneracy is accounted for.

We perform the same splitting of the band indices in $\chi^{\text{2band}}_{abc}$ and $\chi^{\text{3band}}_{abc}$ as we did for the linear response. For $\chi^{\text{2band}}_{abc}$, it is straightforward to obtain the AA approximation as

$$\chi^{\text{2band,AA}}_{abc} = -\frac{ie^3}{\hbar^2 V}\sum_{cv\mathbf{k}}\frac{v^a_{vc}(\mathbf{k})\left\{v^b_{cv}(\mathbf{k})\Delta^c_{cv}(\mathbf{k})\right\}}{\omega^4_{cv}(\mathbf{k})} \times\left[\frac{16}{[\omega_{cv}(\mathbf{k}) - 2\tilde{\omega}]} - \frac{1}{[\omega_{cv}(\mathbf{k}) - \tilde{\omega}]}\right]. \quad (10)$$

However, the effect of the AA approximation on $\chi^{\text{3band}}_{abc}$ is less clear, due to the fact that three bands are now involved. For defining precisely $\chi^{\text{3band,AA}}_{abc}$, we write its vvc terms and the ccv terms [27] as

$$\chi^{\text{3band}}_{abc} = \frac{e^3}{\hbar^2 V}\sum_{v_1v_2c\mathbf{k}}\left[-\frac{\mathcal{F}_{v_1v_2c}}{\omega^3_{cv_1}(\omega_{cv_1}-\omega)} + \frac{\mathcal{F}_{v_1v_2c}}{\omega^3_{cv_2}(\omega_{v_2c}-\omega)} + \frac{16\mathcal{F}_{v_1cv_2}}{\omega^3_{cv_1}(\omega_{cv_1}-2\omega)} - \frac{\mathcal{F}_{v_1cv_2}}{\omega^3_{v_2c}(\omega_{cv_2}-\omega)}\right.$$
$$\left. - \frac{16\mathcal{F}_{cv_1v_2}}{\omega^3_{v_1c}(\omega_{v_1c}-2\omega)} + \frac{\mathcal{F}_{cv_1v_2}}{\omega^3_{v_2c}(\omega_{v_2c}-\omega)}\right] + \frac{ie^3}{\hbar^2 V}\sum_{c_1c_2v\mathbf{k}}\left[\frac{\mathcal{F}_{c_1c_2v}}{\omega^3_{vc_1}(\omega_{vc_1}-\omega)} - \frac{\mathcal{F}_{c_1c_2v}}{\omega^3_{vc_2}(\omega_{c_2v}-\omega)}\right.$$
$$\left. - \frac{16\mathcal{F}_{c_1vc_2}}{\omega^3_{vc_1}(\omega_{vc_1}-2\omega)} + \frac{\mathcal{F}_{c_1vc_2}}{\omega^3_{c_2v}(\omega_{vc_2}-\omega)} + \frac{16\mathcal{F}_{vc_1c_2}}{\omega^3_{c_1v}(\omega_{c_1v}-2\omega)} - \frac{\mathcal{F}_{vc_1c_2}}{\omega^3_{c_2v}(\omega_{c_2v}-\omega)}\right], \quad (11)$$

where we omit the $\mathbf{k}$ dependence for brevity, and

$$\mathcal{F}_{nml}(\mathbf{k}) = \frac{v^a_{nm}(\mathbf{k})\left\{v^b_{ml}(\mathbf{k})v^c_{ln}(\mathbf{k})\right\}}{[2\omega_{ln}(\mathbf{k}) - \omega_{mn}(\mathbf{k})]}. \quad (12)$$

It is now possible to find the antiresonant terms by simply neglecting the terms containing ω_{vc}. Thus,

$$\chi^{\text{3band,AA}}_{abc} = \frac{e^3}{2\hbar^2 V}\sum_{v_1v_2c\mathbf{k}}\left[\frac{\mathcal{F}_{v_1v_2c}}{\omega^3_{cv_1}(\omega_{cv_1}-\tilde{\omega})} - \frac{16\mathcal{F}_{v_1cv_2}}{\omega^3_{cv_1}(\omega_{cv_1}-2\tilde{\omega})} + \frac{\mathcal{F}_{v_1cv_2}}{\omega^3_{v_2c}(\omega_{cv_2}-\tilde{\omega})}\right]$$
$$+ \frac{ie^3}{2\hbar^2 V}\sum_{c_1c_2v}\sum_{\mathbf{k}}\left[\frac{\mathcal{F}_{c_1c_2v}}{\omega^3_{vc_2}(\mathbf{k})[\omega_{c_2v}(\mathbf{k})-\tilde{\omega}]} - \frac{16\mathcal{F}_{vc_1c_2}}{\omega^3_{c_1v}(\omega_{c_1v}-2\tilde{\omega})} - \frac{\mathcal{F}_{vc_1c_2}}{\omega^3_{c_2v}(\omega_{c_2v}-\tilde{\omega})}\right]. \quad (13)$$

To calculate the optical response of a surface we use the slab scheme [28–31]. The slab is composed of N atomic layers [32], having two equivalent surfaces (say, front and back). To this slab, one adds a vacuum region to compose a supercell, that is repeated periodically to fill all the space. The size of the slab and the amount of vacuum are chosen to achieve convergence. The second harmonic generation from the surface is then obtained [31–33] by replacing the velocity matrix element associated with the a direction, that gives the Cartesian direction of the second harmonic polarization, with the modified velocity matrix element given by

$$\mathcal{V}^a_{nm}(\mathbf{k}) = \langle n\mathbf{k}|\frac{\hat{v}^a\mathcal{C}(z) + \mathcal{C}(z)\hat{v}^a}{2}|m\mathbf{k}\rangle, \quad (14)$$

where $\mathcal{C}(z)$ is taken to be 1 for one half of the slab and 0 for the other half, allowing us to select the response from only one (front or back) of the two surfaces of the slab.

III. EFFECTS OF THE ANTIRESONANT APPROXIMATION

In this section we present *ab initio* results for bulk silicon (Si), silicon carbide (SiC), aluminum arsenide (AlAs), gallium arsenide (GaAs), gallium phosphide (GaP), and germanium (Ge) semiconductors which exhibit a zinc-blende structure. We first determine the electronic structure of the material within DFT in the local density approximation (LDA), using norm-conserving Troullier-Martins pseudopotentials and plane-wave basis sets with the ABINIT code [34]. For linear optical spectra, we use the DP code [35].

We performed our calculations for materials containing gallium using a pseudopotential with the electronic configuration $3d^{10}4s^24p^1$. The cutoff energies used are 15 Ha for Si, 30 Ha for SiC, 30 Ha for AlAs, 50 Ha for GaAs, 50 Ha GaP, and 40 Ha for Ge. All materials have been studied with the experimental lattice constant 5.43 Å for Si, 4.36 Å for SiC, 5.66 Å for AlAs, 5.65 Å for GaAs, 5.45 Å for GaP, and 5.66 Å for Ge [20,36]. The spectra for Si, Ge, SiC are obtained using 256 shifted k points in the first Brillouin zone and 864 shifted k points for GaAs, AlAs, and GaP. A broadening of 0.1 eV has been used to smear out the artificial structures due to finite $\mathbf{k}$-point sampling for all materials considered. Finally, crystal local field effects were taken into account by carefully converging the size of the matrices in $(\mathbf{G},\mathbf{G}')$ space using 89 $\mathbf{G}$ vectors for Si, SiC, and Ge, 65 for GaAs, and 59 for AlAs and GaP.

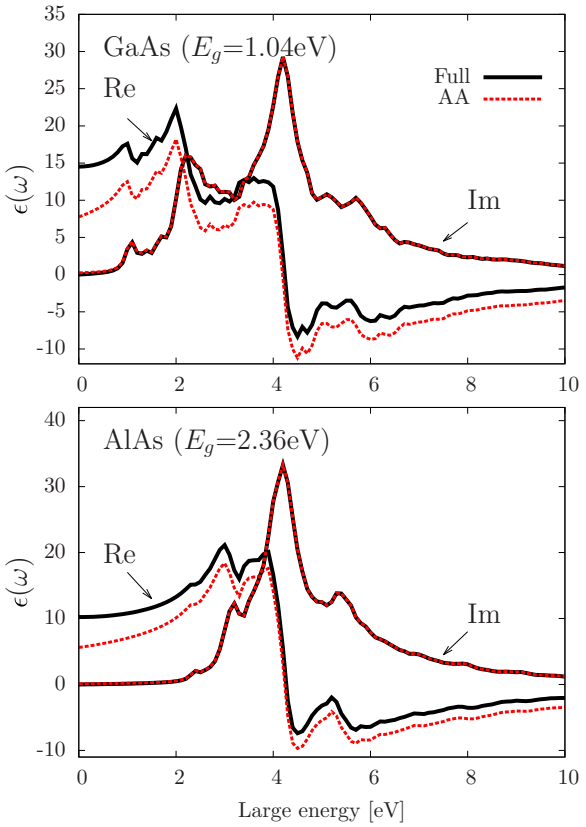

FIG. 1. (Color online) Real and imaginary part of the dielectric function $\epsilon(\omega)$. Solid line: Full *ab initio* calculation; dashed line: AA *ab initio* calculation where the antiresonant term is neglected. E_g is the direct band gap.

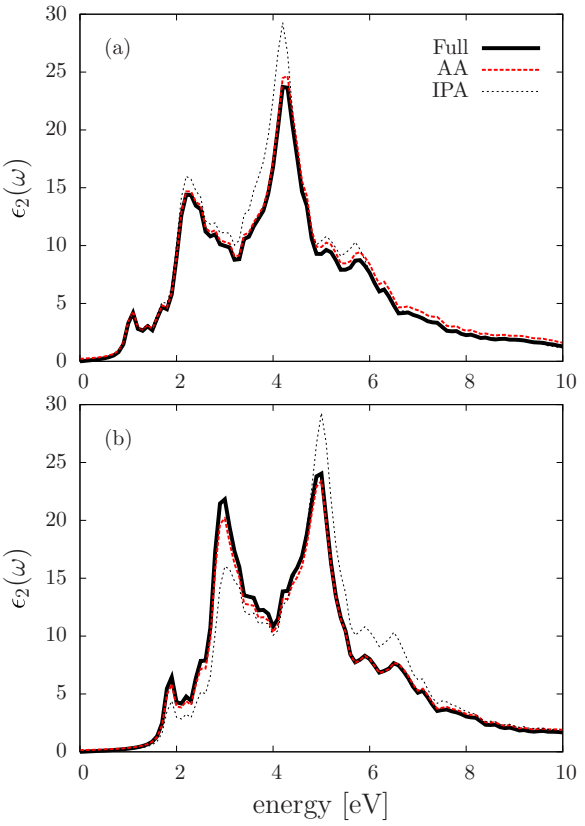

FIG. 2. (Color online) Imaginary part of the dielectric function $\epsilon(\omega)$ for GaAs with (a) local field effects included in the RPA and (b) excitonic effects included using the long-range kernel ($\alpha = 0.2$ [6]) and a scissors of 0.8 eV [6]. Solid line: Full calculation; dashed line: AA calculation where the antiresonant term is neglected; dotted line: IPA calculation as a reference.

A. Linear spectroscopies

1. Optical spectra

In Fig. 1 we show optical spectra obtained for the real and the imaginary part of the dielectric function $\epsilon_{ab}(\omega)$ using Eq. (2) (full calculation, solid lines) and Eq. (3) (AA result, dashed lines), for GaAs and AlAs in the independent particle approximation. Since both bulk GaAs and bulk AlAs are cubic crystals, the dielectric tensor is isotropic [37].

As can be seen from Fig. 1, the imaginary part of dielectric function is unchanged, whereas the real part is different in the AA calculation. The fact that the imaginary part is unchanged can be easily understood by taking the limit $\eta \to 0^+$ in Eqs. (2) and (3). Using the relation

$$\lim_{\eta\to 0^+} \frac{1}{x \pm i\eta} = \mathcal{P}\frac{1}{x} \mp i\pi\delta(x), \tag{15}$$

$\epsilon_2(\omega) = \mathrm{Im}[\epsilon_{ab}(\omega)]$ appears as a collection of δ functions and for positive frequencies contains only a contribution from the resonant part. Here $\mathcal{P}$ denotes the principal value. The nonresonant part does not contribute to the imaginary part of the dielectric function, while the real part is modified.

It is clear that if one is only interested in the optical absorption, proportional to $\epsilon_2(\omega)$, it can be computed exactly under the AA, in the independent particle approximation.

On the other hand, the real part $\epsilon_1(\omega)$ is affected by the approximation. The discrepancy between the full and the AA real part is visible on the entire range of the energy and is particularly important at vanishing frequency. We note that the discrepancy between the two calculations does not disappear at high energy.

As the inclusion of local field and excitonic effects requires the inversion of a matrix, mixing real and imaginary part of $\chi^{(0)}$, we can expect the imaginary part to be in turn affected by the AA, in the presence of local field and many-body effects.

In Figs. 2(a) and 3(a) we report the effect of the AA when local field effects are taken into account using the random phase approximation.

As a matter of fact, absorption spectra when local field effects (solid line) are included do not seem to be affected drastically by the AA (dashed line), for both materials. Moreover, the effect of the AA is negligible compared to the effect of the local fields in itself (see the IPA spectra included for reference, dotted line). We have chosen two semiconducting materials, namely GaAs and AlAs, having different gaps. One can notice that the AA overestimates slightly the absorption of GaAs or AlAs in the main absorption region but this small effect seems to be of the same order of magnitude for both materials. We will analyze later (Sec. III A 3) the link between the gap and the AA on the RPA calculations.

In Figs. 2(b) and 3(b) we present the effect of the AA, when including many-body effects. The screening has been

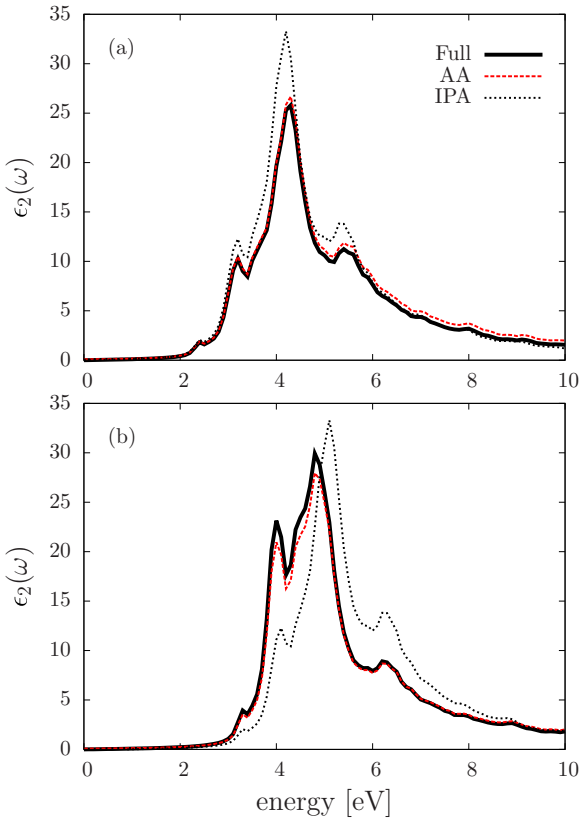

FIG. 3. (Color online) Imaginary part of the dielectric function $\epsilon(\omega)$ for AlAs with (a) local field effects included in the RPA and (b) excitonic effects included using the long-range kernel ($\alpha = 0.35$ [6]) and a scissors of 0.9 eV [6]. Solid line: Full calculation; dashed line: AA calculation where the antiresonant term is neglected; dotted line: IPA calculation for reference.

simulated by applying a scissors operator (SO) and the exciton has been treated thanks to the long-range kernel. In the following we will refer to that calculation as α+SO.

One can notice that the exciton increases the discrepancy between the AA and the full calculation. However, the effect of the inclusion of the exciton is by far more important than the discrepancy introduced by the AA.

The conclusion that comes naturally is that the AA is a good approximation for absorption spectra in the RPA or in the presence of excitonic effects.

We checked also that the modifications of the real part $\epsilon_1(\omega)$, due to the AA, are very similar in the three frameworks IPA, RPA, and α+SO.

2. *Energy loss spectra*

With the aforementioned macroscopic dielectric function ϵ_M, one can obtain electron energy loss spectra (EELS) for vanishing momentum transfer from the loss function $-\mathrm{Im}[1/\epsilon_M(\omega)]$. Obviously, because $-\mathrm{Im}[1/\epsilon_M(\omega)] = \mathrm{Im}[\epsilon_M(\omega)]/\{\mathrm{Re}[\epsilon_M(\omega)]^2 + \mathrm{Im}[\epsilon_M(\omega)]^2\}$, the EELS spectra are expected to be more affected by the AA than the absorption spectra. Moreover, the structure of EELS is mainly given by regions where both the real and the imaginary part are close to zero, corresponding to plasmon frequencies. As it is shown in

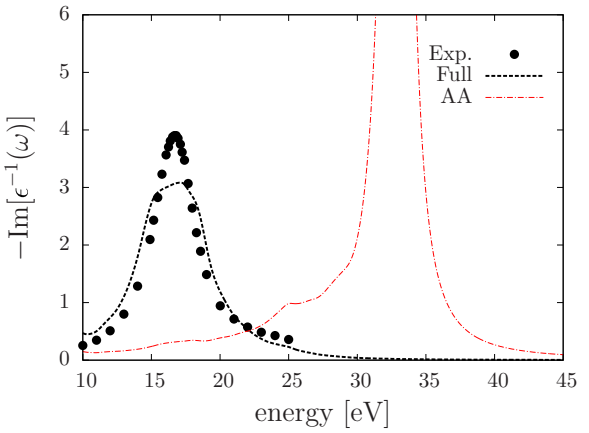

FIG. 4. (Color online) Energy loss function for Si. Dots: Experiment [40]; dashed line: Full RPA calculation; dot-dashed line: AA RPA calculation.

Ref. [38], the RPA already manages to reasonably reproduce the experimental plasmon peak in the case of silicon. Thus, this material appears as a good test case for investigating the validity of the approximation for energy loss spectra.

In Fig. 4 we present the EEL spectrum for bulk silicon. The RPA spectrum compares well with the experimental data (dots, taken from Ref. [6]), while we observe drastic modifications for the RPA spectrum using the AA (dot-dashed line), both in the position and the intensity of the peak. The plasmon frequency has more than doubled, moving from 15.8 to 32.8 eV. Looking more in detail to the real part of the dielectric function, as shown in Fig. 5, one notes that the modifications due to the AA are visible on the entire range of frequencies and strongly affect the position of the zero. The zero of the exact real part results from the cancellation of the two small and slowly decreasing contributions, the resonant and the antiresonant terms. When either one of these two terms is neglected, it leads to an important change in the position of the plasmon frequency.

The second effect of the approximation is the surprising change in intensity of the peak. The f-sum rule concerning the loss function [39] should lead to a AA peak smaller in

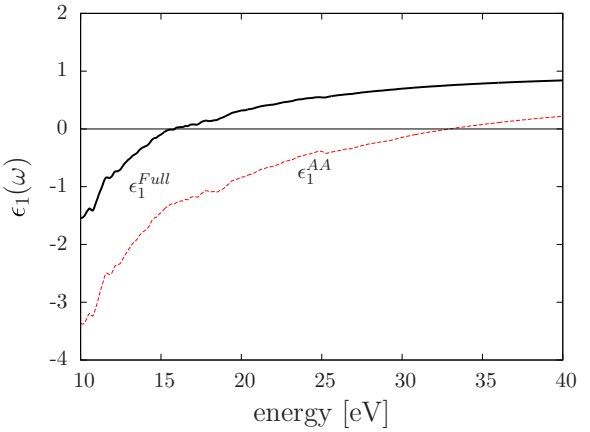

FIG. 5. (Color online) Real part of the dielectric function $\epsilon(\omega)$ for Si. Solid line: Full RPA calculation; dashed line: AA RPA calculation.

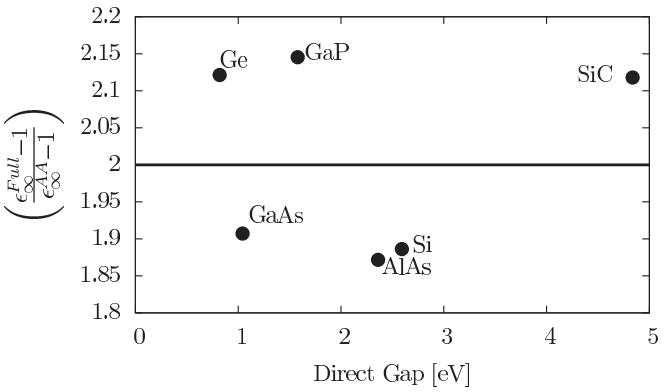

FIG. 6. Effect of the antiresonant approximation on the static dielectric value. Dots represents the RPA values for different materials considered. The solid line represents the ratio obtained analytically for IPA calculations. The direct gap refers here to the DFT direct band gap obtained from the LDA band structure, without applying any scissors operator or GW correction.

intensity, as it is at higher energy. Our results show that sum rules are not fulfilled in the framework of the antiresonant approximation and that the AA is completely inappropriate for energy loss spectra at vanishing momentum.

3. Dielectric constants

In the independent particle approximation (IPA), the effect of the AA on the dielectric constant, obtained at $\omega = 0$ (ϵ_∞), is straightforward because full and AA quantities are related by the relation

$$\left(\frac{\epsilon_\infty^{\text{Full}} - 1}{\epsilon_\infty^{\text{AA}} - 1}\right) = 2. \tag{16}$$

In Fig. 6 we show that this ratio varies as soon as local field effects are included. We previously mentioned that the link between the gap and the accuracy of the AA is not obvious for RPA and α + SO spectra. This is observed and confirmed here. The error introduced in the dielectric constant does not seem to be correlated to the band gap, when local fields are taken into account. The ratio seems to be randomly distributed around the value of 2, independently of the material. These results contradict the general statement telling that small band gap materials are more affected by the AA.

We also want to stress that due to the mixing of the transitions, it is not possible to deduce the correct static value from the AA calculation, making the AA unusable for that purpose. This is illustrated in Table I, for Si, GaAs, and AlAs, in the random phase approximation, including scissors correction (RPA+SO) and the long range kernel for the excitonic effect (α+SO). Smaller values of α are taken from Ref. [6] for correctly reproducing the experimental static values. We see that the antiresonant approximation is far from the expected value for RPA, but the agreement improves when the scissors operator (RPA+SO) and the long range kernel (α+SO) are included.

B. Surface spectroscopy

We exemplify here the effect of the AA on surface spectroscopy using the reflectance anisotropy spectroscopy (RAS). We have checked that the same conclusions hold for the other main surface spectroscopy, namely the surface differential reflectance. The qualitative effects of the AA do not depend on the scheme used to calculate the energies and velocity matrix elements required in Eqs. (1) and (3). Thus, we use a nearest neighbor semiempirical tight-binding (TB) scheme to determined the electronic structure of the surfaces. The TB method, using a $sp^3d^5s^*$ basis set [41,42], gives reliable results and in the case of surfaces we obtain very well converged spectra as a function of the size of the slab, with an easy numerical implementation of the function $C(z)$ described in Sec. II B. Moreover, we have checked for bulk GaAs and AlAs that the conclusions concerning the effect of the AA obtained with the tight-binding and the *ab initio* approaches are the same.

For the surfaces, the Si-Si parameters are taken from Ref. [43] and the H-H and Si-H from Ref. [44]. Intra-atomic matrix elements are important for obtaining quantitative results in TB [45]. As the intra-atomic matrix elements do not exist in the literature for the $sp^3d^5s^*$ basis set, we optimized these parameters, imposing the Thomas-Reiche-Kuhn [46] sum rule to be fulfilled. We also checked that for a smaller basis set (sp^3s^*), we recover the values given by the literature for Si with our approach. The intra-atomic matrix elements used in the surface calculations are given in Table II.

For the clean Si(001)2×1 and dihydride Si(001)1×1:2H surfaces, atomic positions are taken from previous studies (see for instance Ref. [31] and references therein). Supercells are

TABLE I. Static dielectric constants for different materials considered. Values of α are chosen to reproduce the experimental value of the static dielectric constant [6]. IPA values are not shown because the ratio is exactly 2 analytically. Full values are found to be in agreement with previous calculations [6].

	RPA			RPA+SO			α+SO		
Material	Full	AA	$\frac{(\epsilon^{\text{Full}}-1)}{(\epsilon^{\text{AA}}-1)}$	Full	AA	$\frac{(\epsilon^{\text{Full}}-1)}{(\epsilon^{\text{AA}}-1)}$	Full	AA	$\frac{(\epsilon^{\text{Full}}-1)}{(\epsilon^{\text{AA}}-1)}$
Si	12.34	7.012	1.886	11.24	6.376	1.905	12.05	6.592 ($\alpha = 0.09$)	1.976
GaAs	13.13	7.349	1.910	10.67	6.047	1.916	11.05	6.150 ($\alpha = 0.05$)	1.951
AlAs	8.855	5.197	1.872	7.612	4.511	1.883	8.185	4.664 ($\alpha = 0.15$)	1.961

TABLE II. Intra-atomic matrix elements for bulk Si. Other intra-atomic matrix elements are obtained by symmetry. For the surfaces, we used bulk Si intra-atomic matrix elements.

	$\langle s\|d\|p_x\rangle$	$\langle s^*\|d\|p_x\rangle$	$\langle p_x\|d\|d_{xy}\rangle$	$\langle p_x\|d\|d_{3z^2-r^2}\rangle$	$\langle p_z\|d\|d_{3z^2-r^2}\rangle$
Si	0.636	0.247	0.309	0.203	0.258

composed of 32 atomic layers and the spectra are obtained using a 256 off-symmetry **k**-points grid in the 2D Brillouin zone. A smaller broadening of 50 meV has been used to keep track of small structures for reflectance anisotropy spectra.

In Fig. 7 we present the real and imaginary parts of the dielectric function $\epsilon_{yy}(\omega)$ for the two surfaces Si(001)2×1 and Si(001)1×1:2H. Note that the reconstruction induces the presence of surface states in the case of Si(001)2×1. Without the loss of generality, we only show the $\epsilon_{yy}(\omega)$ component [47]. The effect of the AA on the dielectric function appears to be the same as in bulk materials. In particular, the clean surface that exhibits surface states does not seem to be more affected than the dihydride surface.

In Fig. 8 we present the reflectance anisotropy for the case of the clean Si(001)2×1 surface. The reflectance anisotropy is

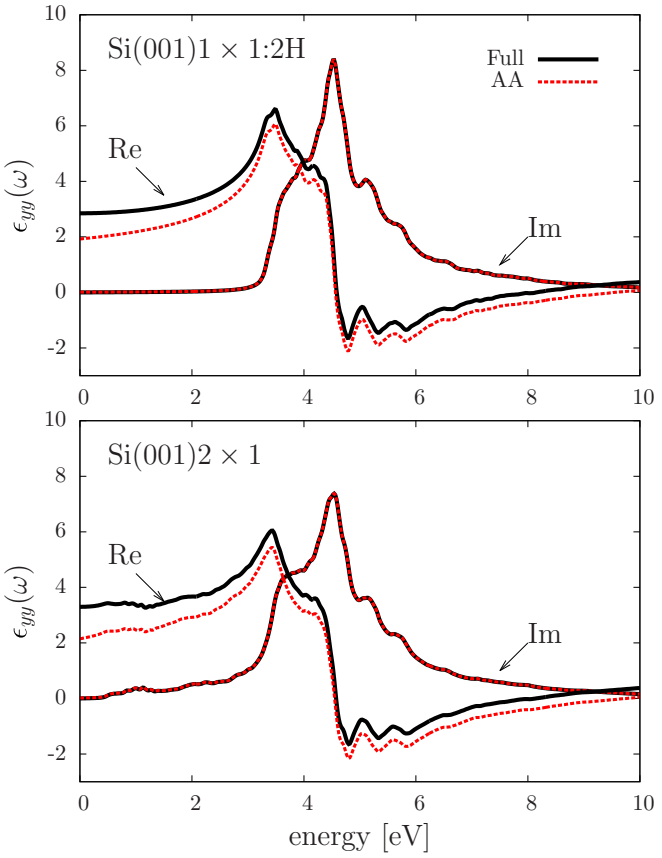

FIG. 7. (Color online) Real and imaginary part of the dielectric function $\epsilon_{yy}(\omega)$. Solid line: Full tight-binding calculation; dashed line: AA tight-binding calculation where the antiresonant term is neglected.

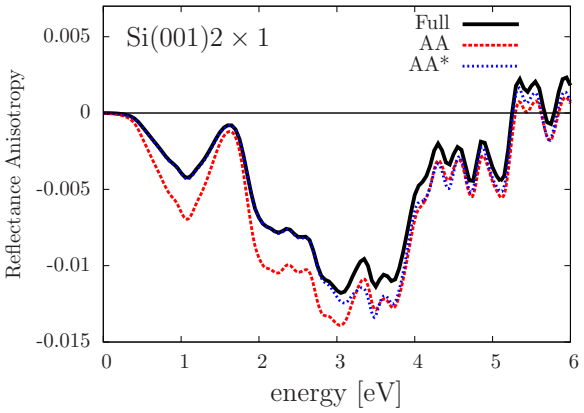

FIG. 8. (Color online) Reflectance anisotropy for the clean Si(001)2×1 surface. Solid line: Full calculation; dashed line: AA calculation where the antiresonant term is neglected. Dotted line: AA* calculation as explained in the text. Spectra have been scaled by a factor as the slab contains two surfaces.

defined as the difference [48]

$$RA = \frac{\Delta R_x(\omega) - \Delta R_y(\omega)}{R_0} = \frac{4\omega}{c}\mathrm{Im}\left(\frac{\epsilon_{xx}(\omega) - \epsilon_{yy}(\omega)}{\epsilon_b(\omega) - 1}\right). \quad (17)$$

As this quantity depends on both the real and imaginary parts of the dielectric functions, it will be affected by the AA. Indeed, one can see that, although the shape of the spectrum is conserved, the reflectance anisotropy differ by 50% around 1 eV. This can be explained by the fact that the reflectance anisotropy is obtained through the difference of two independent quantities, ϵ_{xx} and ϵ_{yy}, that can be affected in a different way by the antiresonant approximation.

In the previous calculation, all the quantities are replaced by their AA counterpart, including the bulk dielectric function. However, the numerical burden is mainly associated with the evaluation of the dielectric response of the surface. An intermediate approach is to compute the RA spectra applying the approximation to the surface calculation only. This less stringent approximation is presented in Fig. 8 and referred as AA* (dotted line). It appears that the AA* spectrum perfectly reproduces the exact spectrum, up to 3 eV. Rewriting slightly Eq. (17), it can be shown that the AA* scheme turns to be exact for the IPA calculation in the gap of the material $\{\mathrm{Im}[\epsilon_b(\omega)] = 0\}$. This is particularly interesting because the RAS focuses mainly on differences occurring at energies in the band gap, where one finds the main differences between different possible reconstructions [48]. As shown previously, the AA is a good approximation for the imaginary part, at any level of sophistication (RPA, α+SO). Thus we expect the RA spectra to be also well approximated with the approximation in the AA* scheme, in presence of local field and excitonic effects, in the low energy range.

C. Second harmonic generation

The experimentally accessible quantity of interest for the second harmonic response is $|\chi_{abc}|$ since neither the real nor the imaginary parts of χ_{abc} have direct and measurable physical meaning separately [49].

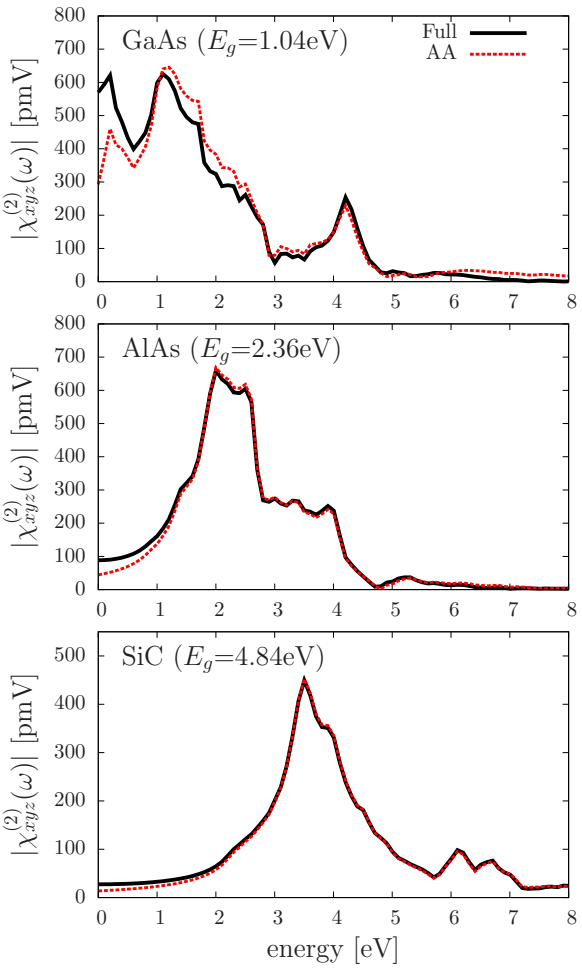

FIG. 9. (Color online) $|\chi_{xyz}|$ and $|\chi^{\mathrm{AA}}_{xyz}|$ for bulk GaAs (top panel), bulk AlAs (middle panel), and SiC (bottom panel). Solid line: Full calculation; dashed line: AA calculation where the antiresonant term is neglected.

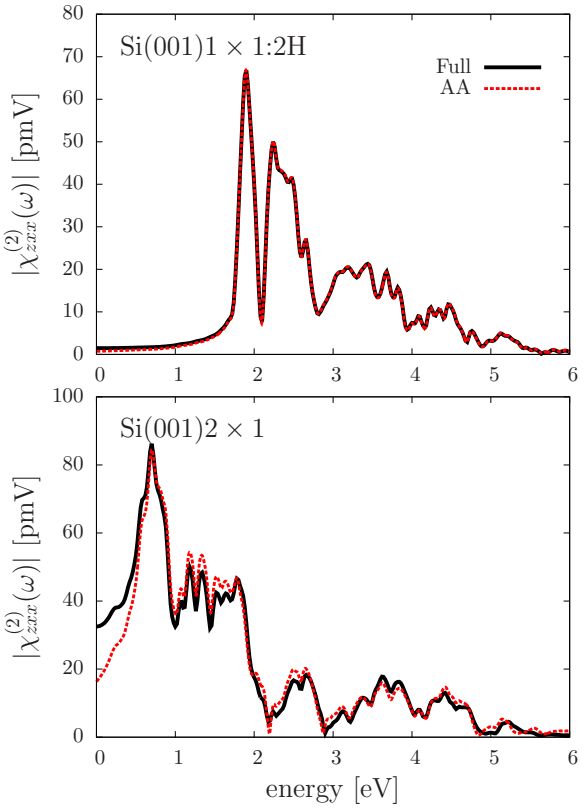

FIG. 10. (Color online) $|\chi_{zxx}|$ and $|\chi^{\mathrm{AA}}_{zxx}|$ for the Si(001)1×1:2H (top panel) and Si(001)2×1 surfaces (bottom panel) from tight-binding calculations. Solid line: Full calculation; dashed line: AA calculation where the antiresonant term is neglected.

Bulk GaAs, AlAs, and SiC have a zinc-blende cubic symmetry, leading to only one nonzero independent tensor component χ_{xyz}. In order to achieve convergence, we used denser grids of 18 522 k points for GaAs and 5488 for AlAs and SiC. The number of conduction bands has also been increased up to 21 conduction bands for all materials. For the two surfaces we present the χ_{zxx} component, where z is the direction perpendicular to the surface. The results for the bulk materials are presented in Fig. 9.

From that figure we readily see that the larger the gap the smaller is the error introduced by χ^{AA}_{abc}. When E_g becomes very small, as in the case of bulk GaAs, the spectra obtained from χ^{AA}_{abc} differs considerably from the full result of χ_{abc}, especially in the low energy range. This is connected again to the fact that, for $\omega = 0$, the value obtained within the approximation is half of the exact value. On the other hand, when E_g is large, as for the silicon carbide, the spectrum obtained from χ^{AA}_{abc} is basically identical to that obtained from χ_{abc}. Moreover, the discrepancy between the two spectra reduces for high energies.

The use of a cut-off function in the calculation of the matrix elements defined in Eq. (14) is mandatory for obtaining a SHG signal from the surface. Thus, the effect of the AA on such systems is an important issue. Results for the surfaces are reported in Fig. 10. The clean Si(001)2×1 surface SHG signal is not properly reproduced, whereas we obtain a reliable SHG spectra for the Si(001)1×1:2H surface. This shows that the conclusions concerning bulk materials also hold for surfaces.

IV. CONCLUSIONS

We have derived the antiresonant approximation for the calculation of the second-order susceptibility. Examples of semiconductors, cubic bulk crystals, and two surfaces, were used to evidence the effects of the approximation on the real and imaginary of the dielectric function and on the loss function. Absorption spectra have shown to be reliably computed under the antiresonant approximation in the RPA or in presence of many-body effects, and to be exact in the IPA. We have shown and explained how energy loss spectra cannot be described by this approximation. The effect of the gap has been discussed, showing that there is no link between the band gap of the materials and the discrepancy between the full and the AA calculations on the dielectric constant. In the case of surfaces, where both the real and imaginary part are needed in the calculation of the reflectance anisotropy, the effect of the AA is more important. But we have presented an

efficient scheme allowing one to use safely the approximation to compute the reflectance anisotropy in the main region of interest, namely in the gap of the material. Finally, we have reported the effect the approximation on second harmonic generation, showing a strong dependence on the band gap for the reliability of the approximation. This limits the range of validity of the approximation for large band gap materials in case of second harmonic generation.

ACKNOWLEDGMENTS

B.S.M. acknowledges the Laboratoire des Solides Irradiés (Ecole Polytechnique, Palaiseau, France) for the support and hospitality during a sabbatical year. B.S.M. acknowledges partial support from CONACYT-México Grant 153930. We would like to acknowledge GENCI (project 544) for the computational support provided.

[1] Y. R. Shen, Nature (London) **337**, 519 (1989).
[2] Y. Takimoto, F. D. Vila, and J. J. Rehr, J. Chem. Phys. **127**, 154114 (2007).
[3] L. Frediani, H. Gren, L. Ferrighi, and K. Ruud, J. Chem. Phys. **123**, 144117 (2005).
[4] J. S. Salafsky, J. Chem. Phys. **125**, 074701 (2006).
[5] G. Onida, L. Reining, and A. Rubio, Rev. Mod. Phys. **74**, 601 (2002).
[6] S. Botti, F. Sottile, N. Vast, V. Olevano, L. Reining, H.-C. Weissker, A. Rubio, G. Onida, R. Del Sole, and R. W. Godby, Phys. Rev. B **69**, 155112 (2004).
[7] J. F. Dobson, *Electronic Density Functional Theory: Recent Progress and New Directions* (Plenum, New York, 1997).
[8] H. Wu, H. Yu, Z. Yang, X. Hou, X. Su, S. Pan, K. R. Poeppelmeier, and J. M. Rondinelli, J. Am. Chem. Soc. **135**, 4215 (2013).
[9] H. Yu, H. Wu, S. Pan, Z. Yang, X. Hou, X. Su, Q. Jing, K. R. Poeppelmeier, and J. M. Rondinelli, J. Am. Chem. Soc. **136**, 1264 (2014).
[10] D. Sangalli, A. Marini, and A. Debernardi, Phys. Rev. B **86**, 125139 (2012).
[11] A. Stroppa, S. Picozzi, A. Continenza, M. Y. Kim, and A. J. Freeman, Phys. Rev. B **77**, 035208 (2008).
[12] M. C. Downer, B. S. Mendoza, and V. I. Gavrilenko, Surf. Interface Anal. **31**, 966 (2001).
[13] F. X. Wang, F. J. Rodriguez, W. M. Albers, R. Ahorinta, J. E. Sipe, and M. Kauranen, Phys. Rev. B **80**, 233402 (2009).
[14] S. A. Yang, X. Li, A. D. Bristow, and J. E. Sipe, Phys. Rev. B **80**, 165306 (2009).
[15] V. I. Gavrilenko, Phys. Rev. B **77**, 155311 (2008).
[16] A. Savoia, D. Paparo, P. Perna, Z. Ristic, M. Salluzzo, F. Miletto Granozio, U. Scotti di Uccio, C. Richter, S. Thiel, J. Mannhart, and L. Marrucci, Phys. Rev. B **80**, 075110 (2009).
[17] B. Fluegel, A. Mascarenhas, J. F. Geisz, and J. M. Olson, Phys. Rev. B **57**, R6787 (1998).
[18] S. Sharma, J. K. Dewhurst, and C. Ambrosch-Draxl, Phys. Rev. B **67**, 165332 (2003).
[19] M. Grüning and C. Attaccalite, Phys. Rev. B **89**, 081102 (2014).
[20] E. Luppi, H. Hübener, and V. Véniard, Phys. Rev. B **82**, 235201 (2010).
[21] S. Sharma and C. Ambrosch-Draxl, Phys. Scr. **2004**, 128 (2004).
[22] C. Attaccalite and M. Grüning, Phys. Rev. B **88**, 235113 (2013).
[23] H.-C. Weissker, J. Serrano, S. Huotari, F. Bruneval, F. Sottile, G. Monaco, M. Krisch, V. Olevano, and L. Reining, Phys. Rev. Lett. **97**, 237602 (2006).
[24] S. Hirata and M. Head-Gordon, Chem. Phys. Lett. **314**, 291 (1999).
[25] F. Sottile, F. Bruneval, A. G. Marinopoulos, L. K. Dash, S. Botti, V. Olevano, N. Vast, A. Rubio, and L. Reining, Int. J. Quantum Chem. **102**, 684 (2005).
[26] R. Leitsmann, W. G. Schmidt, P. H. Hahn, and F. Bechstedt, Phys. Rev. B **71**, 195209 (2005).
[27] E. Ghahramani, D. J. Moss, and J. E. Sipe, Phys. Rev. B **43**, 8990 (1991).
[28] A. Selloni, P. Marsella, and R. Del Sole, Phys. Rev. B **33**, 8885 (1986).
[29] Y.-C. Chang and D. E. Aspnes, Phys. Rev. B **41**, 12002 (1990).
[30] F. Manghi, R. Del Sole, A. Selloni, and E. Molinari, Phys. Rev. B **41**, 9935 (1990).
[31] B. S. Mendoza, F. Nastos, N. Arzate, and J. E. Sipe, Phys. Rev. B **74**, 075318 (2006).
[32] C. Hogan, R. Del Sole, and G. Onida, Phys. Rev. B **68**, 035405 (2003).
[33] B. S. Mendoza, A. Gaggiotti, and R. Del Sole, Phys. Rev. Lett. **81**, 3781 (1998).
[34] X. Gonze, J.-M. Beuken, R. Caracas, F. Detraux, M. Fuchs, G.-M. Rignanese, L. Sindic, M. Verstraete, G. Zerah, F. Jollet, M. Torrent, A. Roy, M. Mikami, P. Ghosez, J.-Y. Raty, and D. Allan, Comput. Mater. Sci. **25**, 478 (2002).
[35] http://www.dp-code.org/
[36] X. Zhu and S. G. Louie, Phys. Rev. B **43**, 14142 (1991).
[37] For zinc-blende cubic symmetry $\epsilon_{xx}(\omega) = \epsilon_{yy}(\omega) = \epsilon_{zz}(\omega) = \epsilon(\omega)$.
[38] V. Olevano and L. Reining, Phys. Rev. Lett. **86**, 5962 (2001).
[39] H. Ehrenreich, in *The Optical Properties of Solids*, Proceedings of the International School of Physics "Enrico Fermi," edited by J. Tauc (Academic Press, New York, 1966), p. 106.
[40] J. Stiebling, Z. Phys. B **31**, 355 (1978).
[41] G. Allan and C. Delerue, Phys. Rev. B **86**, 165437 (2012).
[42] X. Pi and C. Delerue, Phys. Rev. Lett. **111**, 177402 (2013).
[43] Y. M. Niquet, D. Rideau, C. Tavernier, H. Jaouen, and X. Blase, Phys. Rev. B **79**, 245201 (2009).
[44] Y. Zheng, C. Rivas, R. Lake, K. Alam, T. Boykin, and G. Klimeck, IEEE Trans. Electron Devices **52**, 1097 (2005).
[45] A. Miranda, R. Vzquez, A. Daz-Mndez, and M. Cruz-Irisson, Microelectron. J. **40**, 456 (2009), workshop of Recent Advances on Low Dimensional Structures and Devices (WRA-LDSD).
[46] W. Kuhn, Z. Phys. **33**, 408 (1925); F. Reiche and W. Thomas, *ibid.* **34**, 510 (1925).
[47] We have chosen the yy component, since the surface states of Si(001)2×1 are more important along the y axis (defined in crystallographic direction as [110]) which is perpendicular to the dimer direction.
[48] M. Palummo, G. Onida, R. Del Sole, and B. S. Mendoza, Phys. Rev. B **60**, 2522 (1999).
[49] J. E. Sipe and A. I. Shkrebtii, Phys. Rev. B **61**, 5337 (2000).